Effect of bottom argon blowing flow rate on evolution behavior of steel-slag interface

W.-W. Xia [a,c], Q.-Q. Mou [b], Y. Yu [a,c], J.-L. Li [a, b, c, *]

[a] The State Key Laboratory of Refractories and Metallurgy, Wuhan University of Science and Technology, Wuhan, China

[b] CNCEC-EEC Dajiang Environmental Protection Technology Co., LTD., Hubei, Huangshi, China

[c] Key Laboratory for Ferrous Metallurgy and Resources Utilization of Ministry of Education, Wuhan University of Science and Technology, Wuhan, China

* Corresponding author: Jianli Li, E-mail address: jli@wust.edu.cn

(Received 05 December 2024; Accepted 16 May 2025)

Abstract

This research utilizes the computational fluid dynamics (CFD) software FLUENT, which employs the finite volume method, to integrate discrete phase models and multiphase flow models in numerical simulations based on a prototype steel ladle from a particular facility. The simulations aim to investigate the slag entrapment phenomenon in bottom argon blowing. The slag layer is filled with DPM (Discrete Phase Model) particles whose densities are consistent with slag; These particles are used to simulate actual non-metallic inclusions in the slag. When a particle's height is less than the minimum height of the slag layer, it is thought to have been entrained into the molten steel. By using the User Defined Function (UDF), tracking of that particle is stopped. The simulation results reveal that the slag eyes have a tendency to gradually enlarge with increasing argon flow rate. The slag eyes area is generally minor when the argon flow rate is less than 500 L/min; however, there is a noticeable increase in the slag eyes area when the argon flow rate surpasses 1000 L/min. The number of particles entrained into the molten steel increases as the argon flow rate increases; the number of particles entering the steel increases gradually below 1000 L/min and dramatically over 1000 L/min.

Keywords: Numerical Simulation; Discrete Phase; Multiphase Flow; Slag Entrapment; Slag eyes

1 Introduction:

Economic and technological progress have led to an increase in the performance requirements for steel products, which include qualities like stretchability, deep drawability, and low-temperature toughness. Nevertheless, non-metallic inclusions in steel significantly compromise these qualities [1-2]. As a result, metallurgical

companies are working to improve the purity of steel in order to satisfy market demands, utilizing methods like bottom argon blowing in steel ladles, which is an essential secondary refining technique and is widely used in the secondary steelmaking process because of its low equipment requirements, ease of operation, and cost-effectiveness [3]. This technique plays a crucial role in improving the quality of molten steel, reducing inclusions, optimizing the microstructure of the molten steel, adjusting the temperature of the molten steel, and minimizing harmful gases [4-5]. Bottom argon blowing technology is a useful tool for controlling the temperature and composition of molten steel. This reduces the presence of impurities, promotes the deoxidation and desulfurization reactions, and ultimately improves the uniformity and purity of steel [6-9]. Nevertheless, slag entrapment may result from bottom argon blowing. The phenomenon of slag entrapment is mainly caused by the excessive stirring intensity of bottom argon blowing, where surface tension and viscous forces at the steel-slag interface cause portions of the refined slag to form downward drum pack along with the flow of molten steel. Amidst turbulent flows, some of these drum pack detach from the slag layer and, under the influence of surface backflow, are carried into the depths of the melt pool [10]. Some inclusions that float up to the slag-steel interface without being absorbed by the covering slag are re-entrained into the molten steel, or even the surface covering slag is rolled into the interior of the molten steel, causing new contamination. Hence, the rational control of parameters such as argon flow rate, nozzle position, and duration during the bottom argon blowing process in steel ladles is of paramount importance to the quality of the molten steel.

Complications develop during the bottom argon blowing process in steel ladles because of the complex heat transmission and impacts of gas fluid dynamics. The molten steel may be affected by changes in temperature field and gas flow brought on by bottom argon blowing. These changes may result in secondary oxidation, slag entrapment, and steel heat loss from direct air exposure of the molten steel at the slag eyes (the exposed area of molten steel at the steel-slag interface after the slag layer is blown apart). It has been demonstrated that argon stirring is the main source of slag entrapment [6]. Consequently, gaining a profound understanding of the temperature and flow field distributions during bottom argon blowing in the steel ladle, and examining the effects of argon flow rate on diffusion and flow conditions within the molten steel, as well as the size of the slag eyes and slag entrapment in the steel, is of great significance for optimizing the operational parameters of bottom argon blowing and enhancing the quality of the molten steel [11].

The detrimental effect of increasing the gas flow rate over the exposed area of slag eyes, while it helps the mixing within the ladle, has been reported several times in the literature. Several studies have highlighted this trade-off. For instance, Li [12] et al. used a water model and CFD-PBM coupled model to investigate the three-phase flow in a ladle, finding that higher gas flow rates increase the exposed area, which can lead to re-oxidation and other quality issues. Jardón-Pérez [13] et al. demonstrated through physical modeling that an increase in gas flow rate reduces mixing time but also

enlarges the open eye area, leading to potential re-oxidation. Similarly, Mazumdar [14] et al. reported that although a higher gas flow rate decreases mixing time, it increases the slag eye area, making the steel susceptible to re-oxidation. Another study by Jardón-Pérez [15] et al. using PIV measurements confirmed that the optimal gas flow rate must balance the need for efficient mixing with the minimization of the open eye area. These findings emphasize the importance of carefully controlling the gas flow rate to achieve a balance between good mixing and minimizing the exposure of the steel to the atmosphere.

In light of this, Li [16] et al. established a 1:3 scale water model, and through experiments with single-port bottom argon blowing at different positions and flow rates, they concluded that blowing argon at position 2, which is at a 1/2R radius, with a flow rate of 7.6 liters per minute, achieves the best mixing effect while also reducing slag entrapment. Krishnakumar [17] et al. constructed a one-tenth scale steel ladle model at room temperature using a water model and found that the slag eyes size produced by off-center gas injection is smaller than that from center-blowing, and that the viscosity of the slag has little effect on the area of the slag eyes. Inertial and buoyancy effects dominate in determining the size of the slag eyes. Eranandthan [18] et al. also used a water model to conclude that the smaller the density difference between the slag and the molten steel, the easier it is for the slag layer to be entrained into the molten steel, resulting in a larger slag eyes area. Thomas [19] et al. developed a particle capture model based on local force balance and found that increasing the number of particles in the discrete phase model (DPM) can improve the accuracy of particle prediction, with about 97% accuracy achievable with 2500 particles. Amaro-Villeda [20] et al. investigate the impact of slag properties on mixing phenomena within a gas-stirred furnace, utilizing a water model for experimentation. The results revealed that both the thickness and viscosity of the slag can prolong the mixing time, while concurrently reducing the exposed area of the tuyere.

Although bottom argon blowing is essential to secondary refining, issues such slag entrapment and secondary oxidation still exist and have an impact on the stability of molten steel quality. This study offers a scientific foundation for optimizing operations by revealing the effects of bottom argon blowing operational parameters on steel liquid through in-depth investigation and numerical simulation analysis. This research addresses prior limitations relying on qualitative observations by statistically analyzing slag entrapment situations using numerical modeling approaches, employing a steel factory as a case study. The study creates a mathematical model for the steelmaking ladle bottom argon blowing process and uses ANSYS software to predict the flow field distribution and slag entrapment phenomena during the first 300 seconds of bottom argon blowing. Potential consequences during bottom argon blowing can be evaluated based on simulation results, providing a scientific foundation for optimizing these procedures.

2 Mathematical modeling and boundary conditions

2.1 Geometric model

A 1:1 scale model was made, using a prototype steel ladle from a particular steel company. The computational domain was set to include the entire region. The steel ladle measures 4710 mm in total height, 4030 mm for the height of the molten steel region, 50 mm for the thickness of the slag layer, and 630 mm for the height of the top air layer. The diameter of ladle is 4247mm. The nozzle radial position of ladle is 1274.1mm. The two blowing holes have a central angle of 100° and a radius of 130mm for the gas input holes [21-22]. The particular geometric model is displayed in Figure 1(a) and Figure 1(c), where the steel ladle is made up of ladle wall, argon blowing holes, molten steel layer, and slag layer.

The mesh generation of the model was done using the Ansys Meshing program. A hybrid meshing technique was used, creating grids of various densities and sizes from regions with differing degrees of complexity. In order to conserve time and computational resources, this method reduces the number of grids while maintaining computational accuracy. There are roughly 460,000 grids in the ladle model overall. Mesh refinement was used in these regions because of the significant velocity gradient shifts at the gas entrance and slag layer [23-25]. Figure 1(b) displays the outcomes of the mesh generation.

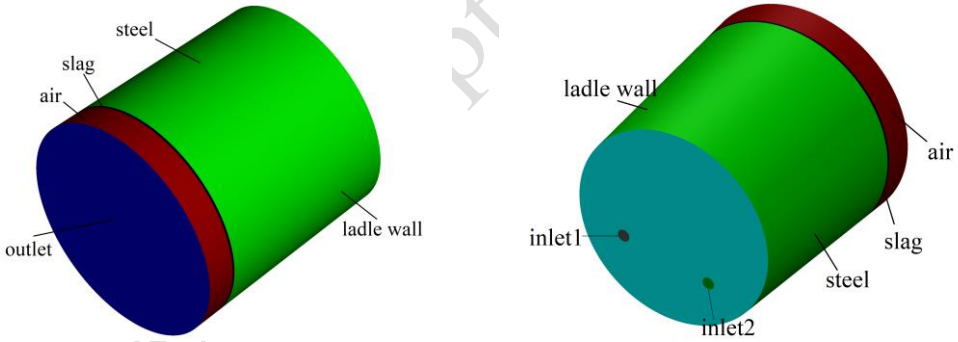

(a)Geometric model

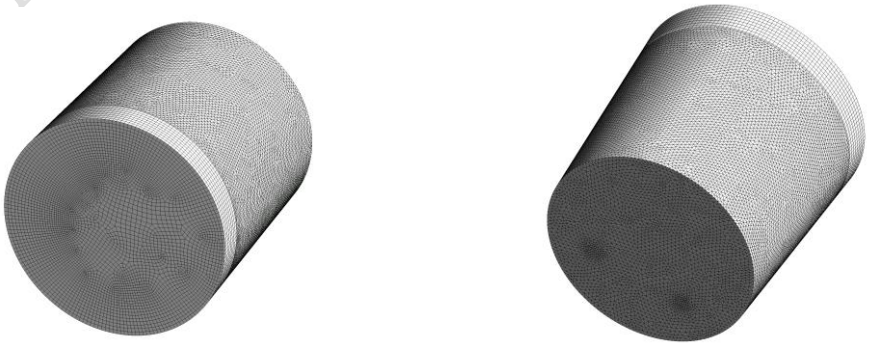

（b）Mesh division

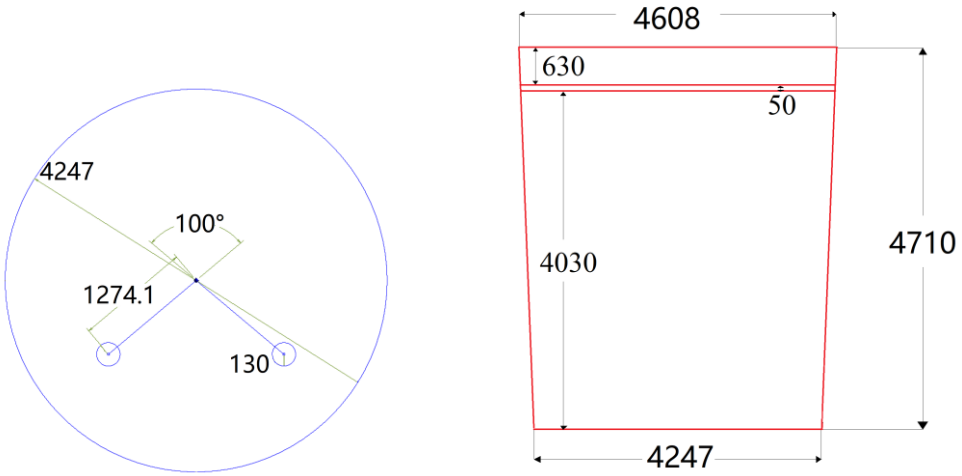

（c）Steel Ladle Design Drawing

Figure 1: Geometric Model of Steel Ladle and Mesh Division

2.2 Fluid model

The model uses the DPM discrete phase model, VOF multiphase flow model, and k-ε realizable model, taking into account computing efficiency and its turbulent viscosity effects [26-29]. There are four phases in the multiphase flow model: slag, molten steel, air, and argon gas.

During bottom argon blowing in the ladle, argon gas is blown into the molten metal bath through argon gas pipes, flow control valves, and pressure regulating valves at the bottom of the ladle [6].The argon gas drives the flow of the molten steel and absorbs impurities from it as it enters the ladle and passes through the molten steel. These contaminants are then transferred to the refining slag at the ladle's top. The solution of continuity, momentum, and energy equations is required for this process, which involves the flow and transport of gas and the transfer of mass, momentum, and energy.

The k-ε realizable equations:

The standard k-ε model was proposed by Launder and Spalding. A key improvement of the realizable k-ε model over the standard k-ε model is the transformation of the turbulent viscosity coefficient μ_t from a fixed constant to a variable that changes with flow conditions. In the standard k-ε model, μ_t is typically set to 0.09, whereas in the realizable k-ε model, it is adjusted according to the flow characteristics, which allows for a better representation of the true nature of turbulent structures in the flow. The realizable k-ε model is particularly suitable for addressing fluid flow problems characterized by strong streamline curvature, vortices, and rotation [30-32]. Therefore, it is employed to track the generation and development of vortices at the steel-slag interface.

$$\frac{\partial}{\partial t}(\rho_l k) + \frac{\partial}{\partial x_j}(\rho_l k u_j) = \frac{\partial}{\partial x_j}\left[\left(\mu + \frac{\mu_t}{\sigma_k}\right)\frac{\partial k}{\partial x_j}\right] + G_k + G_b - \rho_l \varepsilon - Y_M + S_k \qquad (1)$$

$$\frac{\partial}{\partial t}(\rho_l \varepsilon) + \frac{\partial}{\partial x_j}(\rho_l \varepsilon u_j) = \frac{\partial}{\partial x_j}\left[\left(\mu + \frac{\mu_t}{\sigma_\varepsilon}\right)\frac{\partial \varepsilon}{\partial x_j}\right] + \rho_l C_1 S_\tau \varepsilon - \rho_l C_2 \frac{\varepsilon^2}{k + \sqrt{v\varepsilon}} + C_{1\varepsilon}\frac{\varepsilon}{\mathrm{k}} C_{3\varepsilon} G_b + S_\varepsilon (2)$$

Where ρ_l represents the fluid density; k denotes the turbulent kinetic energy; u_j denotes the velocity component in the *j* direction; μ denotes the molecular viscosity. μ_t denotes the turbulent viscosity. σ_ε and σ_k are the Prandtl numbers corresponding to the turbulent kinetic energy and dissipation rate, respectively; G_k is the generation of turbulent kinetic energy due to the gradient of the mean velocity. G_b is the generation of turbulent kinetic energy due to buoyancy. ε is turbulent dissipation rate. Y_M is the contribution of undulating expansion to the overall distribution ratio in compressible turbulence. S_k is user-defined source term, accounting for the effect of external factors on turbulent kinetic energy. C_1、C_2、$C_{1\varepsilon}$ and $C_{3\varepsilon}$ are constants. S_τ is the magnitude of the mean strain-rate tensor. S_ε is user-defined source term, accounting for the effect of external factors on the dissipation rate [33].

In the Volume of Fluid (VOF) model, the scalar phase volume fraction transport equation is solved to track the interface between phases [34]. For the qth phase, its volume fraction equation can be expressed as:

$$\frac{\partial(\rho_l \alpha_q)}{\partial t} + \nabla \cdot (\rho_l \alpha_q u_l) = 0 \quad (3)$$

In the control volume unit, the volume fraction of each phase satisfies:

$$\alpha_a + \alpha_m + \alpha_s = 1 \quad (4)$$

Where *t* represents time; the subscripts *a*, *m*, and *s* respectively indicate the gas phase, steel liquid phase, and slag phase. u_l is the velocity vector of the liquid phase.

The force balance equation for discrete phase particles in the Lagrangian coordinate system is illustrated by Equation (5).

$$m_\mathrm{P}\frac{\mathrm{d}u_\mathrm{P}}{\mathrm{d}t} = m_\mathrm{P}\frac{(u_l - u_\mathrm{P})}{\tau_\mathrm{r}} + m_\mathrm{P}\frac{\mathrm{g}(\rho_\mathrm{P} - \rho_l)}{\rho_\mathrm{P}} + F \quad (5)$$

Where m_P represents the mass of the particle; ρ_P is the density of the particle; u_P is the velocity of the particle ; *F* signifies the additional force including Saffman lift force, virtual mass force, and pressure gradient force; $m_\mathrm{P}\frac{\mathrm{g}(\rho_\mathrm{P}-\rho_l)}{\rho_\mathrm{P}}$ accounts for the particle drag force; and τ_r is the relaxation time of the particle; g is the acceleration due to gravity.

The evaluation index for the particle engulfment rate in the Discrete Phase Model (DPM) is represented by Equation (6).

$$y = \int_0^{300} \frac{\Delta m}{\Delta t} dx \quad (6)$$

Where Δm denotes the change in particle mass, Δt represents the time interval over which the mass change occurs, and *y* signifies the particle engulfment rate in the DPM.

Conservation of mass equation: μ_i represents the viscosity of the liquid phase mixture.

$$\frac{\partial(\rho_l \mu_i)}{\partial x_i} = 0 \tag{7}$$

Momentum conservation equation (Navier-Stokes equation):

$$\frac{\partial}{\partial t}(\rho_l u_i) + \nabla(u_i u_j \rho_l) = -\frac{\partial P}{\partial x_i} + \nabla(\tau) + F_i + \rho_l \mathrm{g} \tag{8}$$

Where P denote the pressure of the fluid, respectively; u_i represents the velocity components of the fluid in the *i* directions; Fi denotes the external forces which in this study include gravity and Surface tension; τ represents the stress tensor.

Energy conservation equation:

$$\frac{\partial(\rho_l e)}{\partial t} + \nabla \cdot (\rho_l e u_l) = -\nabla \cdot q + \tau : \nabla u_l + \rho_l u_l \cdot \mathrm{g} + S \tag{9}$$

Where e denote the Specific total energy (internal energy plus kinetic energy); q denote the Heat flux vector; S denote the Source term, representing other forms of energy input or output.

2.3 Boundary conditions

(1) Inlet velocity condition

The argon intake is configured as a velocity inlet, where the cross-sectional area at the inlet and the gas flow rate is define the velocity magnitude. It is assumed that the velocity distribution is homogeneous over the intake interface and that the velocity at the inlet is perpendicular to the surface. This model adopts dual-port equal gas inlet, and Table 1 reports the flow rate of gas through each inlet port. Empirical formulas are used to determine the turbulent kinetic energy and turbulent dissipation rate at the inlet [35].

$$k_{inlet} = 0.01 v_{inlet}^2 \tag{10}$$

$$\varepsilon_{inlet} = \frac{k_{inlet}^{1.5}}{D_{inlet}/2} \tag{11}$$

Where v_{inlet} is the total velocity of the gas at the inlet; D_{inlet} is the diameter at the inlet. k_{inlet} and ε_{inlet} represent the turbulent kinetic energy and turbulent dissipation rate at the inlet, respectively.

Different blowing stages with specific data are used during argon blowing in the ladle, as shown in table 1.

Table 1: Single Inlet Conditions

Inlet Conditions	1	2	3	4	5
Flow rate, L/min	0	250	500	1000	1500
Velocity, m/s	0	0.03923	0.07846	0.15693	0.23539

(2) Outlet

Set the outlet as a pressure-outlet boundary.

(3) Wall Boundary Conditions

The solid wall surface of the ladle is set as a no-slip wall. This means that the fluid adheres to the wall without slipping, and the fluid velocity gradually decreases as it approaches the boundary layer.

(4) Fluid Property Parameters

The fluid property parameters used in the simulation process are shown in table 2.

(5) Reflux Volume Fraction

Configure the outlet to have a reflux volume fraction of air set to 1, allowing air full backflow.

(6) Gauge Pressure

Set gauge pressure to 0.

Table 2: Fluid Property Parameters

property parameters	argon	slag	molten steel	air
density, kg/m^3	1.6228	3500	7100	1.225
Viscosity, kg/m-s	2.12×10^{-5}	0.31	0.006	1.789×10^{-5}

（7）DPM Particle Parameters

The DPM particle parameters employed in the simulation process are summarized in Table 3.

Table 3: DPM Particle Parameters

property parameters	Density, kg/m^3	Diameter, m	Initial Velocity, m/s
Inert Material	3500	0.0001	0

2.4 DPM settings

To configure the Discrete Phase Model (DPM) in the mathematical model, the following steps were taken:

Activate the Discrete Phase Model (DPM), with the material constituted of an inert material having a density equivalent to that of the slag layer, which is 3500 kg/m³. Enable interactions with the continuous phase and implement unsteady particle tracking.

Set the Injection Type to "volume" and select "slag" in the Zones to enable the generation of DPM particles within the slag layer. Configure the velocity components as follows: The X-direction is defined as the line connecting the centers of the two gas inlet holes, the Y-direction is perpendicular to the line connecting the centers of the gas inlet holes, and the Z-direction is along the height of the ladle. velocity in the x-direction is 0, in the y-direction is 0, and in the z-direction is 0. Set the particle diameter to 0.0001 meters. The injection starts at time 0 second and concludes at time 1 second. To

document the varying mass, utilize the DPM report called mass in domain, which generates files accordingly. Finally, incorporate a User-Defined Function (UDF) using the DEFINE_DPM_TIMESTEP(DPM_TIME, p, ts) macro to delete particles that enter the molten steel at each time step.

2.5 Model Assumptions

1. Assume that the physical properties such as density and viscosity of the steel melt and slag layer are constant. 2. Solidification of the steel melt within the ladle is not considered. 3. Assume that the fluid is at rest at the beginning. 4. The steel melt and refining slag are incompressible fluids. 5. The ladle wall is treated as a no-slip boundary condition. 6. Assume that the inlet velocity distribution of the argon gas is uniform, with the direction being vertically upward. 7. The pore size and position of the permeable brick are known and remain unchanged in the simulation. 8. The actual structural complexities of the ladle are ignored, and it is simplified to an ideal frustum shape.

2.6 Calculation Method for DPM Particle Entrainment Percentage

Excel should be used to open the report file, with a space used as the delimiter. Next, for each row, subtract the current time step time from the next time step time and multiply the result by the current particle mass change. Repeat this process for each row. It can obtain the mass change for each time step.

$$\Delta m_i = (t_{i+1} - t_i) \times \Delta m \tag{12}$$

Where Δm_i represents the mass change for the i-th time step; t_i denotes the time at the current time step; t_{i+1} denotes the time at the next time step; Δm denotes the mass variation at the current time step;

Next, add up the data from each row using the SUM function, which is the amount of slag entrapment.

$$M_{\text{entrapped}} = \int \Delta m_i \tag{13}$$

Where $M_{\text{entrapped}}$ represents the total mass of particles entrapped in the molten steel.

Finally, divide the total particle reduction by the initial total particle mass to find the percentage of particles entrained for various gas flow rates.

$$\text{Percentage of particles entrained} = \left(\frac{M_{\text{entrapped}}}{M_{\text{initial}}}\right) \times 100\% \tag{14}$$

Where M_{initial} represents the initial total mass of particles before any entrapment occurs.

2.7 Mesh Independence

The original model had a mesh count of 800,000. The total mesh count for the ladle was re-divided into 300,000 and 1,200,000, as shown in Figure 2, to compare the surface velocity of the molten steel at an argon gas flow rate of 250 L/min. The surface

velocity of the molten steel is a critical parameter that directly influences key phenomena such as the formation and size variation of slag eyes, the flow field of the molten steel, and the entrainment of inclusions. It is also easily quantifiable, making it convenient for comparison. As shown in Figure 2, when the total mesh counts are 300,000 and 1,200,000, the maximum surface velocities of the molten steel are 0.4680 m/s and 0.5000 m/s, respectively. Compared to the maximum surface velocity of 0.4780 m/s obtained with the mesh count of 800,000 used in this study, the errors are 2.1% and 4.6%, respectively. Thus, the mesh independence was verified.

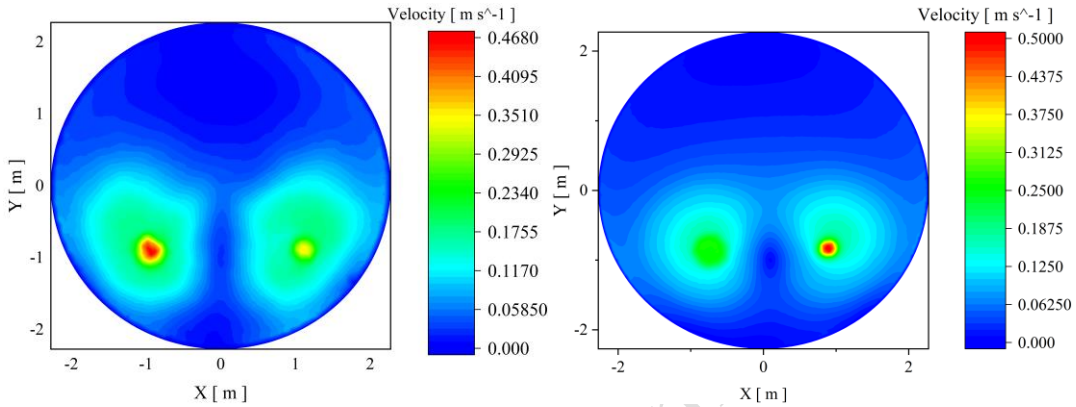

(a)30w-velocity (b)120w-velocity

(c)30w-plane (d)120w-plane

Figure 2: Different Mesh and Results Presentation Plot

3 Results and Discussion

3.1 Analysis of slag eyes condition

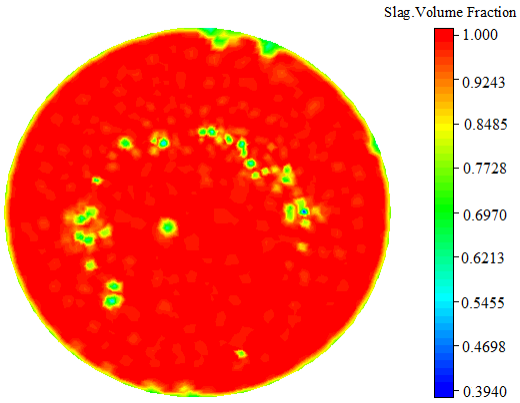

（a）0L/min

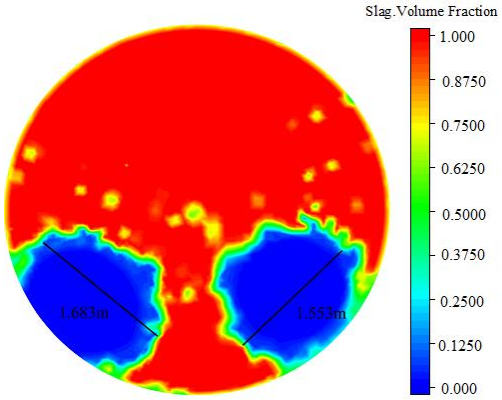

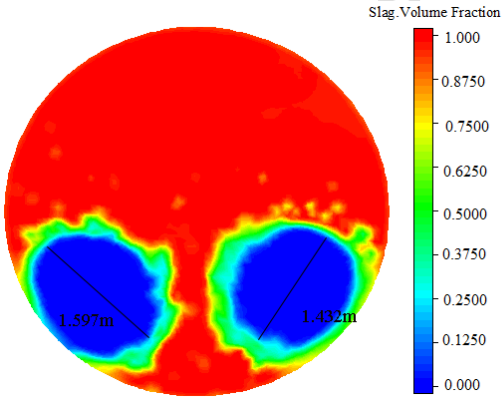

（b）250L/min

（c）500L/min

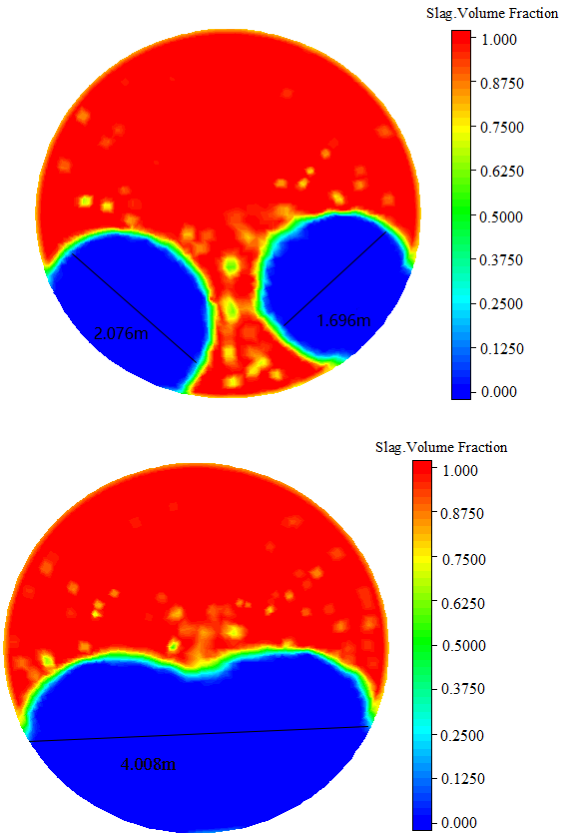

（d）1000L/min （e）1500L/min

Figure 3: Contour map of slag volume fraction in the slag layer at 300 seconds during bottom argon blowing

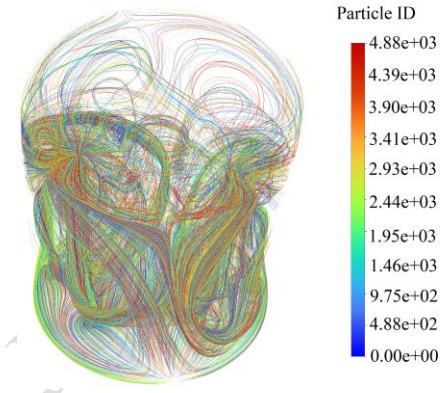

Figure 4: The streamline distribution at 300 seconds in the steel ladle

At a height of 4.08 meters inside the steel ladle, Figure 3 shows the fluctuation in the size of the slag eyes at argon flow rates of 0, 250, 500, 1000, and 1500 L/min. In Figure 4, the streamline diagram within the steel ladle at 300 seconds of argon bottom blowing is depicted alongside the motion trajectories of particles distinguished by their individual IDs, each illustrated in a different colour. Figure 3 clearly illustrates that the area shown is not completely slag when the argon flow rate is 0 L/min because of the randomization in the injection of the discrete phase. With a 250 L/min argon flow rate,

the diameters of the slag eyes are 1.553 and 1.683 meters, respectively. These diameters expand to 1.597 m and 1.432 m when the flow rate reaches 500 L/min. At 1000 L/min, the diameters expand to approximately 2.076m and 1.696m. The area of the slag eyes is significantly larger than when the argon flow rate is 500 L/min. Upon reaching 1500 L/min, the average slag eyes diameter rapidly expands to 2m. The distribution of bubbles widens, with overlapping and intersecting activity zones of multiple bubbles, leading to intersections among slag eyes. An increase in the argon gas flow rate will increase the surface velocity of the molten steel, potentially increasing slag entrapment. An increase in argon flow rate correlates with a gradual enlargement of the slag eyes diameter, as the plume formed by argon bubbles exerts stronger impact on the slag layer [36-38]. When the argon gas flow rate is low, uneven distribution of argon bubbles due to vortex disturbances on the steel surface can reduce the slag eyes diameter, as shown in Figure 3(b). Nonetheless, the general trend indicates an increase in slag eyes diameter with escalating argon flow. During argon blowing, the ascending argon bubbles induce two distinct upward flow streams in the steel, fostering circulation within the ladle (depicted in Figure 4), which facilitates the rise of inclusions to the slag layer, thereby enhancing the removal of impurities from the steel. Simultaneously, this action disrupts surface vortices, mitigating slag entrapment. As the slag eyes area expands, heat loss from the interior of the ladle intensifies, since a larger exposed steel surface accelerates cooling and exacerbates secondary oxidation. The results of this study indicate that in order to decrease the slag eyes area and reduce heat loss, secondary oxidation, and the degree of slag entrapment, it is imperative to keep the argon flow rate below 1000 L/min. Steel quality and process stability are guaranteed by this method.

3.2 Molten Steel Surface Velocity Profile

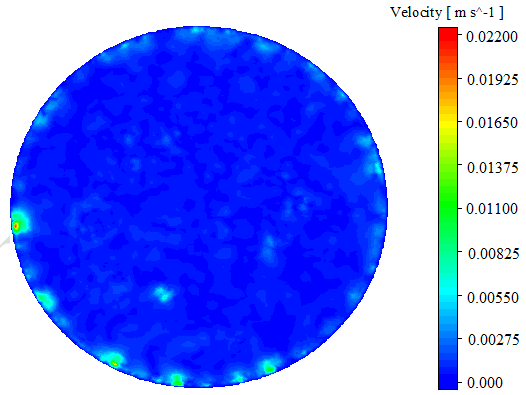

（a）0L/min

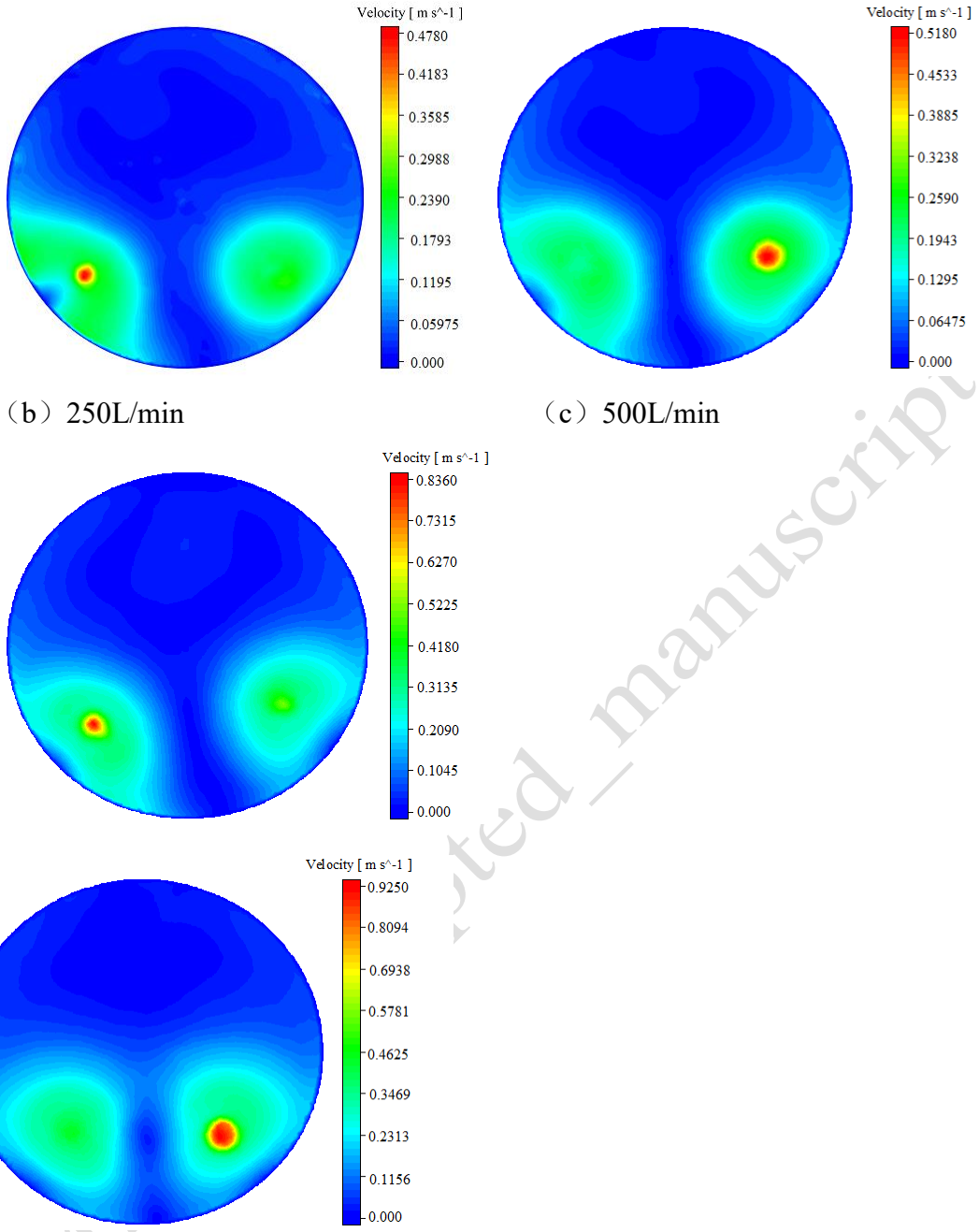

（b）250L/min （c）500L/min

（d）1000L/min （e）1500L/min

Figure 5: Velocity Distribution Contour Map of the Molten Steel Surface at 300 Seconds During Argon Blowing

The molten steel surface velocity profiles in Figure 5 are shown at a height of 3.9 meters inside the steel ladle for argon flow rates of 0, 250, 500, 1000, and 1500 L/min. According to Figure 5, the molten steel has a maximum surface velocity of 0.022 m/s and essentially stays static when the argon flow rate is 0 L/min. Except for a few spots affected by surface tension, the majority of the molten steel surface shows very little flow. The maximum surface velocity of molten steel rises to 0.478 m/s at an argon flow rate of 250 L/min; however, this high velocity is confined to a smaller area. Increasing the argon flow rate to 500L/min elevates the maximum surface velocity of molten steel

increases to 0.518m/s, with a more pronounced increase in the area experiencing higher velocities compared to 250L/min. When the argon gas flow rate escalates to 1000 L/min, the surface velocity of the molten steel dramatically increases to 0.836 m/s, which is considerably higher than the velocity achieved at a flow rate of 500 L/min, accompanied by a significant expansion of the high-velocity region. At 1500L/min, the maximum surface velocity of molten steel further increases to 0.925m/s. Given that the model employs double hole argon blowing with equal flow rates, high-speed argon bubbles ascend, dragging surrounding molten steel and creating two high-velocity zones upon reaching the molten steel surface and penetrating the slag layer. Due to the uncertainties associated with bubble rise and turbulence, the velocity increases when bubbles ascend to a particular area, while it decreases in the absence of rising bubbles. Additionally, the significant variations in velocity on the surface of the molten steel, influenced by turbulence, result in an asymmetric velocity distribution, even when using equal flow rates from two injection points. Conversely, near the steel ladle walls, low-velocity zones form due to resistance offered by the walls. Areas distant from the argon injection points on the steel surface experience lower velocities, lacking direct bubble disturbance. As the argon blowing rate escalates, so does the liquid velocity on the steel surface. However, slag entrapment is governed by both slag drop formation and their subsequent entrapment, and excessively rapid surface velocities can amplify the velocity differential at the slag-steel interface, enhancing the likelihood of slag entrapment [6], thereby impacting the final product quality. Consequently, to prevent excessive surface velocities and the resultant slag entrapment, it is advisable to maintain the argon flow rate below 1000L/min, as inferred from the analysis.

3.3 The analysis of the change in particle quality

The distribution of decreased DPM mass particles in the slag has been statistically examined by numerical simulations; The particle mass change as a result of simulations run at various flow speeds is displayed in Figure 6.

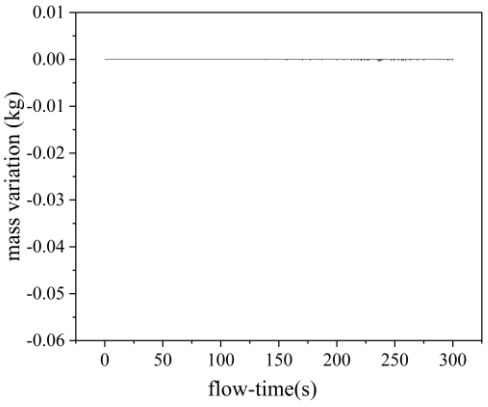

（a）0L/min

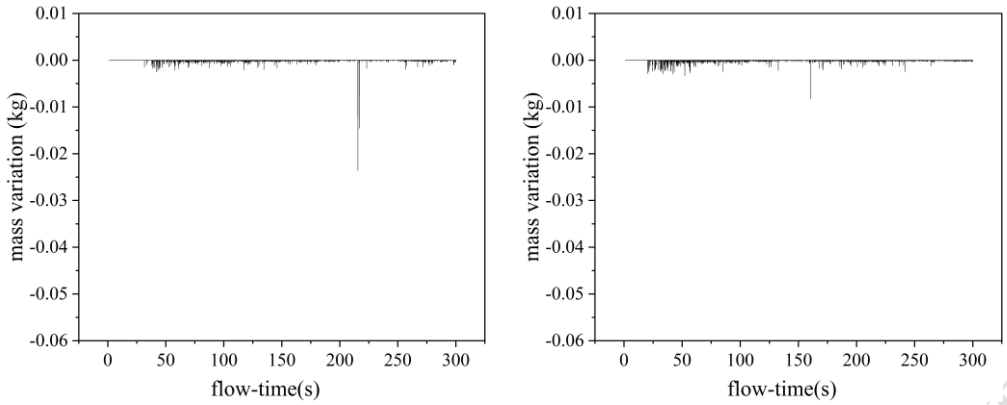

（b）250L/min （c）500L/min

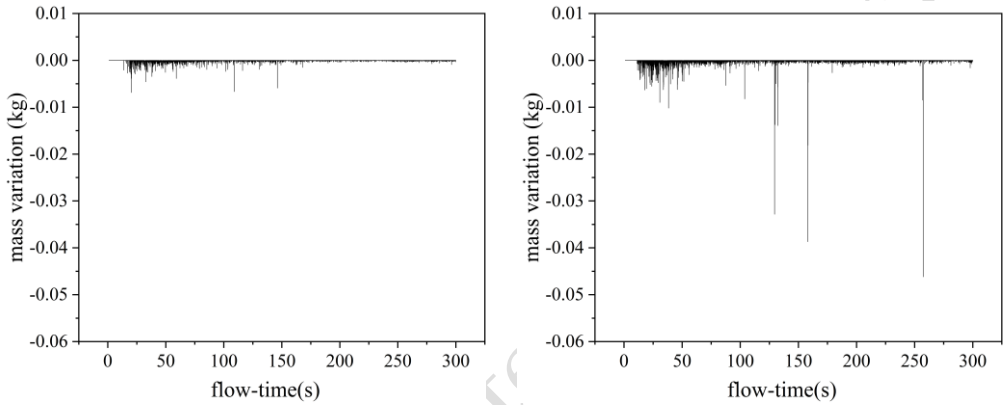

（d）1000L/min （e）1500L/min

Figure 6: Graph of particle mass variation within 300 seconds

With x standing for the current simulation time and y for the change in DPM discrete phase particle mass, Figure 6 shows the variation in DPM particle mass during the length of the simulation, in addition, a review of the Fluent report files reveals that during computation, Fluent removes particles from calculation upon contact with walls and then reinserts them to simulate rebound behavior, which accounts for the variation in particle mass even in the case of zero argon flow. Additionally, in the initial simulation setup, some particles were positioned near the molten steel, naturally settling into the melt steel due to gravity or inertial forces, which explains minor particle entrapment even in the case of zero argon flow.

About the 29th second, very little particulate matter starts to be entrained into the steel melt when the argon flow rate is adjusted to 250L/min. Slag entrapment into the slag occurs at about 25 seconds when the argon flow rate is adjusted to 500L/min, and it occurs earlier and in a significantly larger volume than at 250L/min. Slag entrapment begins at the 20th second with a 1000L/min flow rate, with a larger quantity and at an even earlier time than for 500L/min. Slag entrapment starts as early as the eighth second at a 1500L/min argon flow rate, and all of the slag entrapment volume is enhanced. Because the argon from the bottom has not yet reached the slag layer, the steel surface velocity is kept low. This is why it is noticed that no particles are entrained for a brief

period of time after particle injection stops. Following the cessation of injection, there is a brief period with no particle introduction or entrapment, hence no change in particle mass, reflected by the value of 0 in the graph. Subsequently, as particles are entrained into the melt steel and controlled by the UDF to cease tracking (indicating slag entrapment), particle count decreases, leading to negative values in the curve. The greater the decrease, the more severe the slag entrapment; quantitatively, the number of entrained particles can be calculated through this reduction. Based on these findings, it is recommended that the argon flow rate should be limited to below 1000L/min.

Figure 6 clearly illustrates the relationship between the higher quantity and earlier commencement of slag entrapment and the rise in argon flow rate. To prevent slag entrapment, it is crucial to maintain an argon flow rate below 1000L/min.

3.4 Quantitative analysis of slag entrapment situation

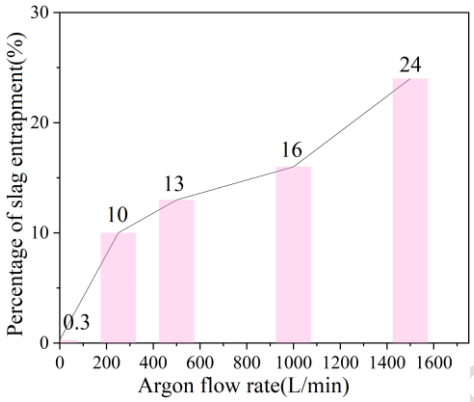

Figure 7: Percentage Chart of Particle Mass Entrapped in the Molten Steel

The mass of particles entrained into the molten steel is shown in Figure 7. Figure 7 shows that when the argon flow rate increases, there is a tendency of increased particle entrapment into the molten steel. Higher argon flow rates produce stronger impact forces and vortex effects, which make it easier for nearby particles to become trapped in the slag layer and give birth to this phenomenon.

As the argon flow rate escalates, argon induces a more potent bubble agitation effect and vortex action [27]. These bubbles and vortices, in turn, mobilize nearby particles, leading to the slag entrapment. With the intensification of the bubble and vortex strength, both the rate and quantity of particle entrapment escalate accordingly. this has implications for the quality of the steel and the refining process. An excessive ingress of particles into the slag layer may undermine its stability, impacting heat transfer and reaction processes within the ladle. Consequently, in practical production, it is crucial to strike a balance in particle entrapment by judiciously controlling the argon flow rate.

Particle entrained in the molten steel increases gradually when the argon flow rate is less than 1000L/min. slag entrapment increases sharply over 1000L/min, though. In light of the previous studies, it is recommended to keep the argon flow rate below 1000L/min in order to preserve the steel melt's quality and the stability of the slag layer.

4 Conclusion

The study examined the effects of argon flow rate on the degree of slag entrapment and the size of the slag eyes by creating a workable three-dimensional transient multiphase mathematical model of the steel ladle. This study led to the following conclusions.

(1) Argon flow rate plays a critical role in controlling slag entrapment. Minimal slag entrapment occurs at around 250L/min. Slag entrapment slightly increases at 500L/min, becomes notable after 20 seconds at 1000L/min, and sharply rises at 1500L/min. To maintain molten steel quality and production efficiency, argon flow rate should be capped at below 1000L/min.

(2) The area of slag eyes grows with increasing flow rate. Relatively small at 250L/min, slightly reduced at 500L/min, they significantly expand at 1000L/min, reducing available space for particles. At 1500L/min, the average diameter reaches 2 meters, with overlap, increasing the risk of particle entrainment. Strict flow rate control is necessary to prevent slag particles from entering the steel melt, argon flow rate should be capped at below 1000L/min.

(3) Surface velocity of the molten steel increases with argon flow. Max velocity is 0.478m/s at 250L/min, 0.518m/s at 500L/min, leaps to 0.836m/s at 1000L/min, and reaches 0.925m/s at 1500L/min, with a larger area experiencing high velocities. To avoid excessive surface velocity of molten steel leading to slag entrapment, argon flow should be maintained below 1000L/min.

Acknowledgments:

We would like to thank Dr. Xiaodong Deng for his valuable advice on statistical analysis. Special thanks to the staff at the Room 721, Steel Building, Wuhan University of Science and Technology for their technical assistance during the experimental phase.

Funding:

This work was financially supported by the National Natural Science Foundation of China (No. 52274341).

Conflict of Interest:

The authors declare that they have no conflict of interest.

Data Availability Statement:

The data generated and analyzed during the current study are not publicly available due to proprietary information but are available from the corresponding author on reasonable request

Author contribution statement:

Conceptualization, Wenwu Xia and Qiqiang Mou; Methodology, Wenwu Xia and Jianli Li; Software, Yue Yu and Wenwu Xia; Validation, Wenwu Xia; Formal Analysis, Wenwu Xia; Investigation, Jianli Li; Data Curation, Wenwu Xia; Writing – Original Draft Preparation, Wenwu Xia; Writing – Review & Editing, Jianli Li; Visualization, Wenwu Xia; Supervision, Jianli Li; Project Administration, Jianli Li; Funding

Acquisition, Jianli Li;

References

[1] C. Liu, X. Gao, S. Ueda, M. Guo, S-Y. Kitamura. Composition changes of inclusions by reaction with slag and refractory: ISIJ International., 60 (2020), 1835-1848. https://doi.org/10.2355/isijinternational.ISIJINT-2019-695.

[2] X. Liu, Q. Jia, C. Liu, A. Xiao, G. Li, Z. He, Q. Wang. Metallurgical mechanism guided machine learning to predict slag entrapment behavior during ladle refining with bottom blowing. Metallurgical and Materials Transactions B. 55 (2024), 1869-1880. https://doi.org/10.1007/s11663-024-03072-8.

[3] M-A. Van Ende, I-H. Jung. A kinetic ladle furnace process simulation model: effective equilibrium reaction zone model using FactSage macro processing. Metallurgical and Materials Transactions B. 48 (2016), 28-36. https://doi.org/10.1007/s11663-016-0698-6.

[4] Y. Zhang, Y. Ren, L. Zhang. Kinetic study on compositional variations of inclusions, steel and slag during refining process. Metallurgical Research & Technology,115 (2018),415. https://doi.org/10.1051/metal/2018059.

[5] H. Hu, L. Yang, Y. Guo, F. Chen, S. Wang, F. Zheng, B. Li. Numerical simulation of bottom-blowing stirring in different smelting stages of electric arc furnace steelmaking.Metals,11 (2021) ,799. https://doi.org/10.3390/met11050799.

[6] J. Li, LF refining technology, Metallurgical Industry Press, Beijing, 2009, pp.10-31. (in Chinese).

[7] Z. Liu, B. Li, A. Vakhrushev, M. Wu, A. Ludwig. Physical and numerical modeling of exposed slag eye in continuous casting mold using Euler–Euler approach. Steel Research International,90 (2018),1-10. https://doi.org/10.1002/srin.201800117.

[8] K. Krishnapisharody, G. A. Irons. A model for slag eyes in steel refining ladles covered with thick slag. Metallurgical and Materials Transactions B, 46 (2014), 191-198. https://doi.org/10.1007/s11663-014-0184-y.

[9] S. Chatterjee, K. Chattopadhyay. Physical modeling of slag ‘eye’ in an inert gas-shrouded tundish using dimensional analysis. Metallurgical and Materials Transactions B.47 (2015), 508-521. https://doi.org/10.1007/s11663-015-0512-x.

[10] L. Han, X. Li, Y. Liu. Water model experiment of 70t bottom-blown argon ladle. Laboratory Research and Exploration,30 (2011), 29-34. https://kns.cnki.net/kcms2/article/abstract?v=W694F5cljyBRjrq3JEwoPR5aHVSxP-UU1zmFY-T7ChPJyty6SXfM10QprrnyybgENz7KnhWgNVG3X4bBmvIRFB24irrV0WSvS5wJoL62Y_kwzgLCbtElCgpf-acDk_fqa4qdy8fLF0fcArIBC6hscZPYGVAWcz7yYqY3W2MNxYyoDIeVLTaBVQTBiuyO8c-Z&uniplatform=NZKPT&language=CHS (in Chinese).

[11] Song, J., Zhang, J.-m., Yin, Y.-b., & Zhen, X.-g. Optimizing power-saving process for a 120-t ladle furnace. Journal of Iron and Steel Research International, 32(3) (2024), 594-605. doi:10.1007/s42243-024-01320-4.

[12] Linmin, L., Zhongqiu, L., Baokuan, L., Hiroyuki, M., & Fumitaka, T. Water

model and CFD-PBM coupled model of gas-liquid-slag three-phase flow in ladle metallurgy. ISIJ International, 55(7) (2015), 1337-1346. doi:10.2355/isijinternational.55.1337.

[13] Jardón-Pérez, L. E., González-Morales, D. R., Trápaga, G., González-Rivera, C., & Ramírez-Argáez, M. A. Effect of differentiated injection ratio, gas flow rate, and slag thickness on mixing time and open eye area in gas-stirred ladle assisted by physical modeling. Metals, 9(5) (2019),555. doi:10.3390/met9050555.

[14] Dipak, M., Palani, D., & Rajagopal, S. Modeling and optimisation of gas stirred ladle systems. ISIJ International, 57(2) (2017), 286-295. doi:10.2355/isijinternational.ISIJINT-2015-701.

[15] Jardón Pérez, L. E., Amaro-Villeda, A., Conejo, A. N., González-Rivera, C., & Ramírez-Argáez, M. A. Optimizing gas stirred ladles by physical modeling and PIV measurements. Materials and Manufacturing Processes, 33(8) (2017), 882-890. doi:10.1080/10426914.2017.1401722.

[16] Z. Li, W. Ouyang, Z. Wang, R. Zheng, Y. Bao, C. Gu. Physical simulation study on flow field characteristics of molten steel in 70t ladle bottom argon blowing process. Metals,13 (2023),639. https://doi.org/10.3390/met13040639.

[17] K. Krishnapisharody, G. A. Irons. Modeling of slag eye formation over a metal bath due to gas bubbling. Metallurgical and Materials Transactions B, 37 (2006), 763-772. https://doi.org/10.1007/s11663-006-0058-z.

[18] M. Eranandhanthan, D. Mazumdar. Modeling of slag eye area in argon stirred ladles. ISIJ International.,50 (2010), 1622–1631. https://doi.org/10.2355/isijinternational.50.1622.

[19] B. G. Thomas, Q. Yuan, S. Mahmood, R. Liu, R. Chaudhary. Transport and entrapment of particles in steel continuous casting. Metallurgical and Materials Transactions B,45 (2013), 22-35. https://doi.org/10.1007/s11663-013-9916-7.

[20] Amaro-Villeda, A. M., Ramirez-Argaez, M. A., & Conejo, A. N. Effect of slag properties on mixing phenomena in gas-stirred ladles by physical modeling. ISIJ International, 54(1) (2014), 1-8. doi:10.2355/isijinternational.54.1.

[21] X. Guo, J. Godinez, N. J. Walla, A. K. Silaen, H. Oltmann, V. Thapliyal, A. Bhansali, E. Pretorius, C. Q. Zhou. Computational investigation of inclusion removal in the steel-refining ladle process. Processes, 9 (2021),1048. https://doi.org/10.3390/pr9061048.

[22] Z. Tan, Y. Yu, X. Deng, J. Li. Simulation analysis of influence of argon gas injection hole position on flow field in steel ladle. JOM, (2024), 6925–6933. https://doi.org/10.1007/s11837-024-06415-7.

[23] G. Wang, G. Cheng, Y. Zhang, L. Chen, L. Hui, Q. Wang, H. Cai. Numerical and physical simulation of mixing process in argon-stirred ladles with single and dual bottom injection. JOM, (2024), 4572–4586. https://doi.org/10.1007/s11837-024-06618-y.

[24] F. Su, L. Fang, Z. Kang, H. Zhu. Numerical simulation on heat transfer of multi-layer ladle in empty and heavy condition. Frontiers in Heat and Mass Transfer., 20

(2023),1-
9.doi:10.5098/hmt.20.14.https://cdn.techscience.cn/uploads/attached/file/20230425/20230425161938_89003.pdf.

[25] Y. Liu, H. Bai, H. Liu, M. Ersson, P. G. Jönsson, Y. Gan. Physical and numerical modelling on the mixing condition in a 50t ladle.Metals,9 (2019),1136. https://doi.org/10.3390/met9111136.

[26] X. Li, B. Li, Z. Liu, R. Niu, Y. Liu, C. Zhao, C. Huang, H. Qiao, T. Yuan. Large eddy simulation of multi-phase flow and slag entrapment in a continuous casting mold.Metals,9 (2018),7. https://doi.org/10.3390/met9010007.

[27] W. Liu, H. Tang, S. Yang, M. Wang, J. Li, Q. Liu, J. Liu. Numerical simulation of slag eye formation and slag entrapment in a bottom-blown argon-stirred ladle. Metallurgical and Materials Transactions B, 49 (2018), 2681-2691. https://doi.org/10.1007/s11663-018-1308-6.

[28] L. Wang, J. Yang, Y. Liu. Numerical investigation for effects of polydisperse argon bubbles on molten steel flow and liquid slag entrapment in a slab continuous casting mold. Metallurgical and Materials Transactions B, 53 (2022), 3707-3721. https://doi.org/10.1007/s11663-022-02634-y.

[29] X. Li, B. Li, Z. Liu, D. Wang, T. Qu, S. Hu, C. Wang, Gao R. Evaluation of slag entrapment in continuous casting mold based on the les-vof-dpm coupled model. Metallurgical and Materials Transactions B, 52 (2021), 3246-3264. https://doi.org/10.1007/s11663-021-02253-z.

[30] G. Chen, Q. Wang, S. He. Assessment of an eulerian multi-fluid VOF model for simulation of multiphase flow in an industrial Ruhrstahl–Heraeus degasser. Metallurgical Research & Technology, 116 (2019),617.doi: 10.1051/metal/2019049.

[31] A. Gupta, R. Kumar, R. K. Singh. Assessment of critical vortexing height to prevent slag entrapment during tundish teeming. Metals and Materials International, 28 (2021), 1246-1256. https://doi.org/10.1007/s12540-021-01014-6.

[32] X. Zhao, J. Zhang, F. Gao, X. Wang, L. Wang. Transient simulation of slag entrapment in a tundish. Journal of Physics: Conference Series, 2390 (2022),012080.doi: 10.1088/1742-6596/2390/1/012080.

[33] Aydogdu, M. Analysis of the effect of rigid vegetation patches on the hydraulics of an open channel flow with Realizable k-ε and Reynolds stress turbulence models. Flow Measurement and Instrumentation, 94 (2023), 102477. doi:10.1016/j.flowmeasinst.2023.102477.

[34] R. D. Morales, S. Garcia-Hernandez, J. D. J. Barreto, A. Ceballos-Huerta, I. Calderon-Ramos, E. Gutierrez. Multiphase flow modeling of slag entrapment during ladle change-over operation. Metallurgical and Materials Transactions B, 47 (2016), 2595-2606.https://doi.org/10.1007/s11663-016-0663-4.

[35] Xufeng, Q. Study on gas-liquid two phase flow behavior under effects of annular gas curtain and swirling flow at tundish nozzle. (Doctoral dissertation, Wuhan University of Science and Technology, Wuhan, Hubei, 2021, P.R. China). Retrieved from https://link.cnki.net/doi/10.27380/d.cnki.gwkju.2021.000533. (in Chinese)

[36] A. Srivastava, K. Chattopadhyay. Macroscopic mechanistic modeling for the prediction of mold slag exposure in a continuous casting mold. Metallurgical and Materials Transactions B, 53 (2022), 1018-1035. https://doi.org/10.1007/s11663-021-02396-z.

[37] Wang, N., Liu, Z., Li, C., & Li, B. Effect of differential flow blowing argon on mixing time and slag eye in dual nozzle ladle by numerical simulation. Metallurgical and Materials Transactions B, 55(4) (2024), 2240-2257. doi:10.1007/s11663-024-03088-0.

[38] He, Y., Liu, J., Su, X., Li, W., Pan, Y., & Wang, D. Characteristics of bubble behavior and inclusion removal in liquid steel based on industrial trials of argon injection into ladle shroud. Metals, 13(3) (2023),593. doi:10.3390/met13030593.

Table captions in this article:

Table 1. Single Inlet Conditions.

Table 2. Fluid Property Parameters.

Table 3. DPM Particle Parameters.

Figure captions in this article:

Figure 1. Geometric Model of Steel Ladle and Mesh Division.

Figure 2. Different Mesh and Results Presentation Plot.

Figure 3. Contour map of slag volume fraction in the slag layer at 300 seconds during bottom argon blowing.

Figure 4. The streamline distribution at 300 seconds in the steel ladle.

Figure 5. Velocity Distribution Contour Map of the Molten Steel Surface at 300 Seconds During Argon Blowing.

Figure 6. Graph of particle mass variation within 300 seconds.

Figure 7. Percentage Chart of Particle Mass Entrapped in the Molten Steel.